NANO LETTERS
Letter
pubs.acs.org/NanoLett

Continuously Controlled Optical Band Gap in Oxide Semiconductor Thin Films

Andreas Herklotz,*,† Stefania Florina Rus,*,‡ and Thomas Zac Ward*,†

†Materials Science and Technology Division, ORNL, Bethel Valley Road, Oak Ridge, Tennessee 37831-6056, United States
‡Renewable Energies Laboratory - Photovoltaics, National Institute for Research and Development in Electrochemistry and Condensed Matter, Timisoara 300569, Romania

Supporting Information

ABSTRACT: The optical band gap of the prototypical semiconducting oxide SnO_2 is shown to be continuously controlled through single axis lattice expansion of nanometric films induced by low-energy helium implantation. While traditional epitaxy-induced strain results in Poisson driven multidirectional lattice changes shown to only allow discrete increases in bandgap, we find that a downward shift in the band gap can be linearly dictated as a function of out-of-plane lattice expansion. Our experimental observations closely match density functional theory that demonstrates that uniaxial strain provides a fundamentally different effect on the band structure than traditional epitaxy-induced multiaxes strain effects. Charge density calculations further support these findings and provide evidence that uniaxial strain can be used to drive orbital hybridization inaccessible with traditional strain engineering techniques.

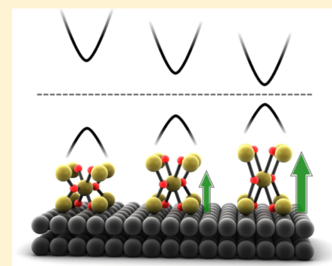

KEYWORDS: *Strain doping, tin oxide, helium ion implantation, ellipsometry, uniaxial strain*

Band gap engineering is a common and powerful technique for tuning properties of group IV and III−V semiconductors.[1−4] However, oxides' inherent chemical and thermal stability are beginning to make them the preferred candidates for many next generation alternative energy technologies where the ability to finely control band gap energies is critically tied to functionality.[5,6] For example, simple binary oxides like CoO[7] and TiO_2[8] as well as more complex systems like perovskite $SrTiO_3$[9] or spinel Co_3O_4[10] have each been investigated for their promise as photocatalysts in photoelectrochemical hydrogen production through water splitting. However, the majority of oxide semiconductors have band gaps well above the visible spectrum, which poses serious limitations to photovoltaic and photocatalytic applications where a high absorption across the solar spectrum is desired to maximize efficiency. Finding ways to control and optimize band gaps of oxides without deteriorating secondary properties is thus a critical need to bring oxides into mainstream application. Various strategies have been developed and applied successfully but have their limitations. The creation of localized states through doping with nonisovalent ions has been shown to be an effective route in reducing the band gap[11−14] but comes at the cost of a decrease of energy conversion efficiency through charge trapping. Alloying[15−18] or codoping[19] are alternative approaches that are generally less critical in terms of trap state creation but are more complex or limited to the specific material system. As band structures of oxide semiconductors are often particularly sensitive to changes in bond angles and bond length, strain has been suggested as a general means to tailor band alignments without the introduction of trap sites.[20−24] Practically, strain in thin films is usually imposed by the heteroepitaxial growth on nonlattice-matched substrates. This method involves perturbation in all three unit cell dimensions because the in-plane (ip) strain induced into a film's lattice is accommodated by an elastic reaction along the out-of-plane (oop) lattice direction driven by the Poisson effect. In addition, traditional heteroepitaxial biaxial strain has only shown the ability to change band gaps in a discrete manner and is severely limited by the availability of suitable substrates. Unlike conventional epitaxy-based strain tuning methods, strain doping a lattice by implanting noble helium atoms into an epitaxial oxide film was recently shown to be an effective means of continuously controlling lattice expansion along the oop axis while leaving the ip axes locked to the substrate.[25] Functionality could then be controlled through orbital polarization of the 3d electrons without noticeable defect generation in the film. Importantly for photoresponsive functionalities, this method allows continuous control over a material's electronic character without the requirement of electron doping through alloying, which can generate charge trapping centers.

In this work, we show that strain doping can be extended to transparent semiconductors and that He implantation can be used to tailor band gaps of oxides. We demonstrate that the structural and optical properties of high-quality epitaxial SnO_2 films can be finely controlled using He implantation and that the impact of uniaxial out-of-plane strain is fundamentally different than biaxial in-plane strain by providing detailed density functional theory (DFT) analysis comparing these

Received: November 25, 2015
Revised: January 23, 2016

ACS Publications © XXXX American Chemical Society

DOI: 10.1021/acs.nanolett.5b04815
Nano Lett. XXXX, XXX, XXX−XXX

systems. Further, we show that uniaxial strain provides access to orbital states not available through epitaxy-induced strain engineering and thus presents a new and compelling path to study the fundamental response of optostructural properties of oxide semiconductors.

SnO_2 films of 15 nm thickness have been grown by pulsed laser deposition on an (0001) oriented single-crystalline sapphire substrate using a stoichiometric target. The growth temperature and laser energy was 700 °C and 2.0 J/cm^2, respectively. The growth has been carried out in an oxygen pressure of p_{O_2} = 50 mTorr and the films were annealed for 20 min and cooled down in 0.5 atm O_2 to ensure a good oxygen stoichiometry. After deposition, 15 nm thick Au buffer layers were sputtered onto the SnO_2 films. He implantation was carried out ex situ with 4 keV He ions using a commercial ion gun. The Au buffer layers were removed afterward. The penetration depth of He into the perovskite lattice is in the order of 35 nm at 4 keV.[26] Thus, He is implanted across the entire 15 nm thick film. However, we note that the He distribution is not homogeneous and hence a strain gradient is present in the SnO_2 film after He dosing. This strain gradient is small enough not to affect the main messages of our study, as will be discussed later.

The as-grown and He-dosed films have been characterized by X-ray diffraction. Details on the structural characterization can be found in the Supporting Information. All films are single-crystalline with a SnO_2 [010]//$Al_2O_3\langle 11\bar{2}0\rangle$ epitaxial relationship that is consistent with previous results.[27−29] The a, b, and c lattice parameter of the as-grown film has been determined from 2θ scans on ip and oop reflections to be 4.71, 4.78, and 3.21 Å, respectively. The lattice parameters are close to that of bulk SnO_2 ($a_{bulk} = b_{bulk}$ = 4.73 Å and c_{bulk} = 3.19 Å[30]). The large lattice mismatch of 13.8% along the c-axis results in almost complete strain relaxation. A small residual tensile ip strain is present that slightly reduces the oop lattice parameter versus the bulk lattice.

Figure 1 shows θ−2θ scans along the 200 reflection of the SnO_2 films with increasing He dose. Dosing the film with He gradually shifts the 200 film peak to smaller angles as expected for a linear increase of the out-of-plane lattice parameter a. This demonstrates that He implantation allows for an excellent fine control of out-of-plane strain. A maximal oop lattice expansion of about 1.7% is reached for the 10 × 10^{15} He/cm^2 dosed film. The film peak slightly broadens upon He implantation that is merely an effect of the slight variation in strain rather than a decreased film quality due to disorder. The inhomogeneous He distribution across the film thickness is typical for ion implantation processes and consequently leads to a small strain distribution across the film's thickness. Additionally, short-range lattice distortions that are restricted to the close proximity of the He sites may contribute to the small broadening of the XRD peak. On the basis of previous work,[25] we estimate that even the highest dose presented results in an occupation of only about 1 He/130 unit cells. If we would consider that a substantial part of the strain propagation was short-range, we should therefore see a "double peak" comprised of a broad and diffuse XRD peak due to the highly strained region and another unstrained region that would resemble the XRD peak of the undosed film. However, it can clearly be observed that the full film peak is shifting in the XRD scans. This means that a coherent lattice distortion, that is, the

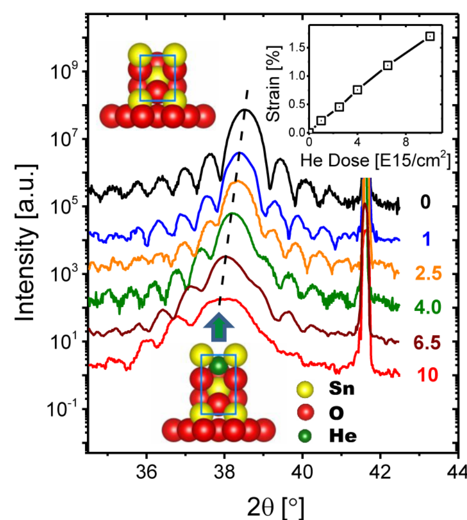

Figure 1. Structural characterization: θ−2θ scans around the 200 SnO_2 reflection of films with increasing He dose. The inset shows the out-of-plane strain in respect to the undosed film calculated from the film peak positions in dependence of the He dose. The schemes illustrate the uniaxial expansion along the out-of-plane axis introduced by He implantation.

result of long-range elastic forces induced by He incorporation, is dominant.

Laue oscillations remain observable for all doses, which indicate that the structural quality of the film is not deteriorated. The low energy of the He used during implantation is well below the threshold for generation of lattice defects, such as oxygen vacancies.[31] The Au buffer further reduces the energy of He and prevents sputtering effects to the SnO_2 film. This is important to note, because lattice defects can create states well within the band gap and thus seriously affect optical properties. In order to show that the crystalline film quality is not reduced during He implantation, XRD rocking curves around the 200 film reflections are shown in Figure 2 for the undosed (left) and 10 × 10^{15} He/cm^2 dosed

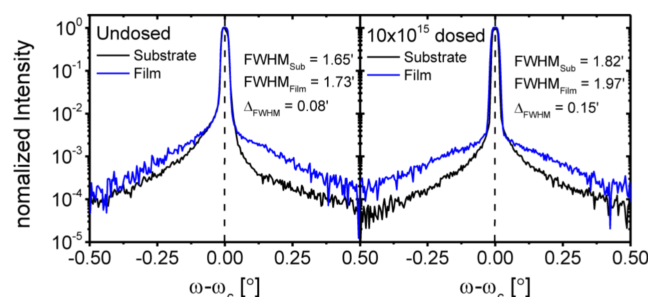

Figure 2. Rocking curves on the 200 SnO_2 film and 0006 sapphire substrate reflections before (left) and after dosing with 10 × 10^{15} He/cm^2 (right). The enhancement of the rocking curve width upon He implantation is within the error of the measurement.

film (right), respectively. The as-grown films possess excellent oop epitaxy with the rocking curve widths only about 0.1−0.2′ larger than the substrate. The width of the rocking curve is unchanged after implantation within the error of the measurement, which indicates that the epitaxy is not affected and that no substantial concentration of lattice defects is generated. Atomic force microscopy (AFM) images of the undosed and dosed films (see Supporting Information) reveal an atomically

DOI: 10.1021/acs.nanolett.5b04815
Nano Lett. XXXX, XXX, XXX−XXX

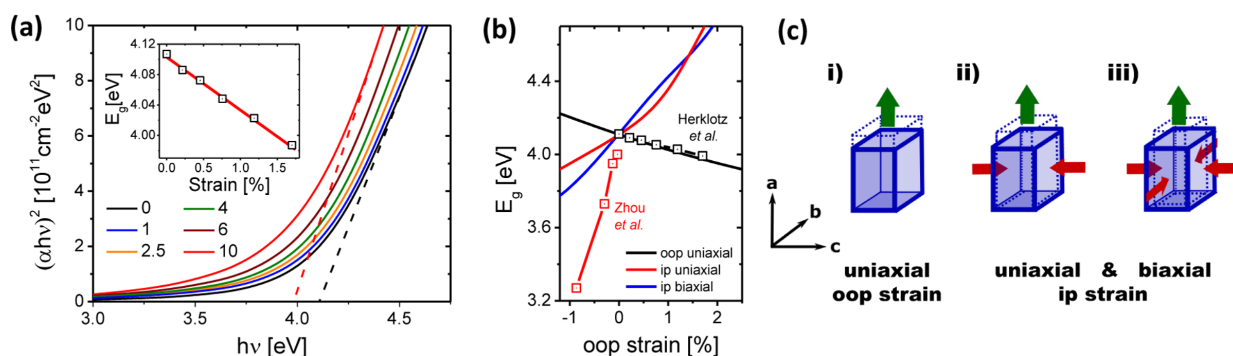

Figure 3. Optical properties of He implanted SnO_2. (a) Optical band gap change as determined by the linear extrapolation of the absorption coefficient α in the $(\alpha h\nu)^2$-Tauc plot. The inset shows the band gap in dependence on the He dose. (b) Band gap as a function of oop strain calculated by DFT (dashed lines). Experimental data on uniaxial oop strain from this study (black symbols) and uniaxial ip strain published by Zhou et al.[27] (red symbols) is shown for comparison. (c) Schematics of the three different strain scenarios that are discussed.

flat surface with a root-mean-squared roughness of 0.1−0.2 nm. This proves that ion sputtering effects are limited to the first few nanometers of the Au cap layer and the atomically flat SnO_2 surface is revealed after the removal of the cap layer.

Two facts should be stressed before continuing to the next part of the discussion. First, He implantation induces uniaxial strain by expanding the oop lattice while the ip lattice remains fixed with respect to the substrate. This has been shown conclusively for coherently grown $La_{1-x}Sr_xMnO_3$ films.[25] It holds true also for strain-relaxed oxide films because due to the epitaxy to the substrate an in-plane lattice expansion could only be imposed by plastic deformation via defect generation or motion. However, at room temperature defects in oxides are generally immobile. Confirmation of the uniaxial lattice expansion of the SnO_2 films upon He implantation can be found in the Supporting Information. Second, it should be pointed out that due to the nobility of He the implantation does not change the electronic state directly unlike conventional doping mechanisms.

The optical properties of the SnO_2 films have been determined by variable angle spectroscopic ellipsometry (VASE). The data have been recorded in the energy range 1.2 to 5.0 eV and have been fitted to a simple two-layer model consisting of the substrate and film. This is a reasonable simplification considering the following statements: (i) the substrate−film interface and film−air surface are atomically flat and render the introduction of intermediate model layers unnecessary; (ii) the He doping level variation across the film thickness is small enough that the film can be approximated as a single layer with homogeneous optical constants (see Supporting Information); and (iii) He that passes the SnO_2 film and ends up in the substrate has a negligible influence on the optical properties of sapphire because it is a wide band gap material (E_g = 9.9 eV) with low absorption over the full spectroscopic range. Neutral point defects, such as He in a corundum structure, generally contribute very little to light scattering and will increase absorption only insignificantly.[32] For this reason, the optical constants of the sapphire substrates have been determined by a VASE measurement on the bare substrate and have been fixed in the two-layer model system. The SnO_2 layer was fitted by a Kramers−Kronig consistent B-spline model. In Figure 3a, we show the $(\alpha h\nu)^2$ Tauc-plot of the optical absorption spectrum for all films with varied He dose. This plot allows for the determination of direct optical band gaps by extrapolating the linear parts of the curves to zero. The inset presents the band gap dependence on strain. The band gap is linearly decreasing with a change of about −1.5% per 1% lattice expansion. Thus, strain doping through He implantation is shown to be capable of continuously controlling optical band gaps.

In the following, we discuss the response of the band gap to strain. Figure 3b shows the band gap as a function of the oop strain (black open symbols) in comparison to density functional theory calculations (DFT, solid lines) and previous experimental results by Zhou et al.[27] (red open symbols). Interestingly, the band gap change for the latter is considerably larger than found for single axis oop strain and of different sign. This indicates that biaxial in-plane compressive strain driving oop expansion and uniaxial oop expansion have fundamentally different effects on the electronic band structure. A release of tensile ip strain, as studied by Zhou et al., increases the oop lattice constant a and decreases the band gap, while uniaxial strain by He implantation increases a as well, but drives the band gap into the opposite direction. The band gap dependence thus seems to be more complex with the introduction of Poisson effects.

In order to discuss this behavior, we calculated the change of the electronic band gap under different strain scenarios using DFT. We differentiate three cases which are illustrated in Figure 3 (c). In case (i), the oop lattice parameter is increased, whereas the ip parameter are fixed. This is analogous to the uniaxial increase of oop strain by He implantation in epitaxial a-oriented SnO_2 films. In cases (ii) and (iii), ip strain is applied, while the oop lattice is free to elastically react to the imposed stress. This is the common situation in epitaxial thin film growth. Uniaxial ip strain (case (ii) can occur in systems where the lattice mismatch along one direction is so small that coherent growth is achieved while strain relaxation occurs along the other direction due to a larger lattice mismatch. This situation is found for SnO_2 films grown on (0001)-oriented sapphire and was discussed by Zhou et al. In case (iii), symmetric biaxial strain was considered. This situation is commonly found for heterogrowth of films with a quadratic ip lattice, for example, growth on cubic materials.

For the DFT calculations, the pseudopotential Quantum ESPRESSO code was deployed. First, geometric optimization of the rutile bulk structure was carried out using the Perdew−Burke−Ernzerhof (PBE) exchange functional within the generalized gradient approximations (GGA). The results have been found to be satisfactorily converged for a plane-wave energy cutoff of 80 Ry and a 4 × 4 × 6 k-point grid. The optimized SnO_2 structure has the lattice parameters a_{the} = 4.78

DOI: 10.1021/acs.nanolett.5b04815
Nano Lett. XXXX, XXX, XXX−XXX

Å and c_{the} = 3.21 Å, which are only slightly larger than the experimental lattice parameters. The overestimation is typical for GGA calculations. After the determination of the stress-free bulk structure orthorhombic distortions according to (i)−(iii) were applied. In order to get reliable band gap values, the hybrid PBE0 functional has been applied for the final DFT calculation after structural relaxation within the given constraints. Hybrid functionals incorporate a portion of exact exchange from Hartree−Fock theory and thus correct for the well-known underestimation of band gaps for simple ab initio functionals. Here we tune the Hartree−Fock portion to match the electronic band gap of the relaxed structure with the experimentally determined optical band gap.

The band gaps as a function of the oop strain determined by our DFT calculations are shown as solid lines in Figure 3b. Our result on uniaxial oop strain (black line) is in excellent agreement with the decrease of the band gap experimentally observed by He implantation. We also point out that our calculated response to uniaxial oop strain is different in sign and magnitude compared to the band gap change for uniaxial and biaxial ip strain. These results show that the band gap of SnO_2 critically depends on the type of strain applied to the unit cell. They also demonstrate that uniaxial oop strain induced by He implantation offers a fundamentally different approach to strain tailoring of band gaps compared to the common practice of thin film epitaxy.

Our calculations indicate that in each strain scenario roughly two-third of the strain-induced band gap change is attributed to the shift of the conduction band minimum (CBM), while only one-third is coming from the change of the valence band maximum (VBM). To gain further insight into the origin of the different strain response, we have calculated the charge density distribution at the VBM and CBM. Figure 4 shows the distribution at a tensile oop strain of +4% where the band gap differences are large and the charge distribution differences are most noticeable. In agreement with previous publications,[27,33−35] we find that the VBM consists entirely of O 2p states. Differences between the different strain types are rather small. However, the differences in the CBM charge density are more pronounced. The CBM is composed of hybridized O 2p and Sn 5s states. While the O orbitals are more of 2p character for the two ip strain scenarios, hybridization is strongly enhanced under uniaxial oop strain. The latter leads to a reduction of the CBM energy and thus, a lower band gap compared to the two other strain scenarios.

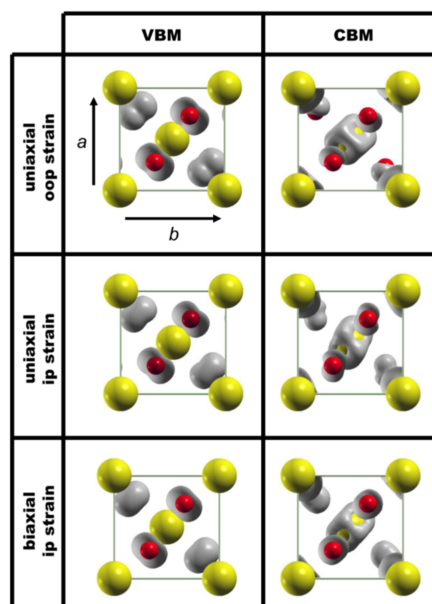

Figure 4. Calculated charge density distribution under +4% oop strain at the VBM and the CBM for the three different strain scenarios. The isosurface was set to 0.004 e/Å^3.

In summary, we report the use of low-energy He implantation as a means to tune the optical band gap in epitaxial films of the prototypical oxide semiconductor SnO_2. We find that this method allows for fine control of uniaxial out-of-plane strain that results in a continuously tunable band gap. The responses predicted by density functional theory closely match the observed relation of decreasing band gap with uniaxial lattice expansion while demonstrating that there exists a fundamental difference in how electronic structure responds to uniaxial and traditional multiaxes strain engineering. Calculated charge density distributions are also presented that demonstrate that uniaxial strain provides access to orbital states not available through epitaxy-induced strain engineering. These results demonstrate that strain doping offers an exciting new approach to the fundamental study of strain-dependent properties in oxides. The ability to tailor valence and conduction band states without significant introduction of the typical charge trapping defect states present with electron/hole doping techniques may lead to significantly improved efficiencies and new levels of tunability in many functionally relevant applications.

■ ASSOCIATED CONTENT

Supporting Information

The Supporting Information is available free of charge on the ACS Publications website at DOI: 10.1021/acs.nanolett.5b04815.

Structural characterization, film morphology before and after He implanation, ellipsometry models, optical properties, and additional figures and references. (PDF)

■ AUTHOR INFORMATION

Corresponding Authors

*E-mail: herklotza@gmail.com.
*E-mail: rusflorinastefania@gmail.com.
*E-mail: wardtz@ornl.gov.

Notes

The authors declare no competing financial interest.

■ ACKNOWLEDGMENTS

This effort was wholly supported by the U.S. Department of Energy (DOE), Office of Basic Energy Sciences (BES), Materials Sciences and Engineering Division, with user projects supported at ORNL's Center for Nanophase Materials Research (CNMS), which is also sponsored by DOE-BES.

■ REFERENCES

(1) Capasso, F. *Science* **1987**, *235*, 172−176.
(2) Greil, J.; Lugstein, A.; Zeiner, C.; Strasser, G.; Bertagnolli, E. *Nano Lett.* **2012**, *12*, 6230−6234.
(3) Hong, K.; Kim, J.; Lee, S.-H.; Shin, J. K. *Nano Lett.* **2008**, *8*, 1335−1340.
(4) Lyons, D. M.; Ryan, K. M.; Morris, M. A.; Holmes, J. D. *Nano Lett.* **2002**, *2*, 811−816.

DOI: 10.1021/acs.nanolett.5b04815
Nano Lett. XXXX, XXX, XXX−XXX

(5) Balachandran, P. V.; Rondinelli, J. M. *Nat. Commun.* **2015**, *6*, 6191.
(6) Wang, F.; Grinberg, I.; Rappe, A. M. *Appl. Phys. Lett.* **2014**, *104*, 152903.
(7) Liao, L.; et al. *Nat. Nanotechnol.* **2013**, *9*, 69−73.
(8) Asahi, R.; Morikawa, T.; Ohwaki, T.; Aoki, K.; Taga, Y. *Science* **2001**, *293*, 269−271.
(9) Modak, B.; Ghosh, S. K. *J. Phys. Chem. C* **2015**, *119*, 23503−23514.
(10) Qiao, L.; Xiao, H. Y.; Meyer, H. M.; Sun, J. N.; Rouleau, C. M.; Puretzky, A. A.; Geohegan, D. B.; Ivanov, I. N.; Yoon, M.; Weber, W. J.; Biegalski, M. D. *J. Mater. Chem. C* **2013**, *1*, 4628−4633.
(11) Yu, W.; Jiang, K.; Wu, J.; Gan, J.; Zhu, M.; Hu, Z.; Chu, J. *Phys. Chem. Chem. Phys.* **2011**, *13*, 6211−6222.
(12) Choi, W. S.; Chisholm, M. F.; Singh, D. J.; Cho, T.; G, E. J., Jr.; Lee, H. N. *Nat. Commun.* **2012**, *3*, 689.
(13) Grinberg, I.; West, D. V.; Torres, M.; Gou, G.; Stein, D. M.; Wu, L.; Chen, G.; Gallo, E. M.; Akbashev, A. R.; Davies, P. K.; Spanier, J. E.; Rappe, A. M. *Nature* **2013**, *503*, 509−512.
(14) Egdell, R. G. *Springer Ser. Surf. Sci.* **2015**, *58*, 351.
(15) Scanlon, D. O.; Regoutz, A.; Egdell, R. G.; Morgan, D. J.; Watson, G. W. *Appl. Phys. Lett.* **2013**, *103*, 262108.
(16) Jahangir-Moghadam, M.; Ahmadi-Majlan, K.; Shen, X.; Droubay, T.; Bowden, M.; Chrysler, M.; Su, D.; Chambers, S. A.; Ngaii, J. H. *Adv. Mater. Interfaces* **2015**, *2*, 1400497.
(17) Cho, S.; Jang, J. W.; Zhang, W.; Suwardi, A.; Wang, H.; Wang, D.; MacManus-Driscoll, J. L. *Chem. Mater.* **2015**, *27*, 6635.
(18) Harunsani, M. H.; Oropeza, F. E.; Palgrave, R. G.; Egdelll, R. G. *Chem. Mater.* **2010**, *22*, 1551.
(19) Comes, R. B.; Sushko, P. V.; Heald, S. M.; Colby, R. J.; Bowden, M. E.; et al. *Chem. Mater.* **2014**, *26*, 7073.
(20) Schlom, D. G.; Chen, L.-Q.; Fennie, C. J.; Gopalan, V.; Muller, D.; Pan, X.; Ramesh, R.; Uecker, R. *MRS Bull.* **2014**, *39*, 118−130.
(21) Yin, W.-J.; Chen, S.; Yang, J.-H.; Gong, X.-G.; Yan, Y.; Wei, S. *Appl. Phys. Lett.* **2010**, *96*, 221901.
(22) Shao, R.-W.; Zheng, K.; Wei, B.; Zhang, Y.-F.; Li, Y.-J.; Han, X.-D.; Zhang, Z.; Zou, J. *Nanoscale* **2014**, *6*, 4936−4941.
(23) Walsh, A.; Catlow, C. R. A.; Zhang, K. H. L.; Egdell, R. G. *Phys. Rev. B: Condens. Matter Mater. Phys.* **2011**, *83*, 161202.
(24) Sushko, P. V.; Qiao, L.; Bowden, M.; Varga, T.; Exarhos, G. J.; Urban, F. K.; Barton, D.; Chambers, S. A. *Phys. Rev. Lett.* **2013**, *110*, 077401.
(25) Guo, H.; Dong, S.; Rack, P. D.; Budai, J. D.; Beekman, C.; Gai, Z.; Siemons, W.; Gonzalez, C. M.; Timilsina, R.; Wong, A. T.; Herklotz, A.; Snijders, P. C.; Dagotto, E.; Ward, T. Z. *Phys. Rev. Lett.* **2015**, *114*, 256801.
(26) Autier-Laurent, S.; Plantevin, O.; Lecoeur, P.; Decamps, B.; Gentils, A.; Bachelet, C.; Kaitasov, O.; Baldinozzi, G. *Europhys. Lett.* **2010**, *92*, 36005.
(27) Zhou, W.; Liu, Y.; Yang, Y.; Wu, P. *J. Phys. Chem. C* **2014**, *118*, 6448.
(28) Tien, L. C.; Norton, D. P.; Budai, J. D. *Mater. Res. Bull.* **2009**, *44*, 6−10.
(29) Ke, C.; Yang, Z.; Zhu, W.; Pan, J. S.; Karamat, S. *J. Appl. Phys.* **2010**, *107*, 013515.
(30) Peercy, P. S.; Morosin, D. *Phys. Rev. B* **1973**, *7*, 2779.
(31) Livengood, R.; Tan, S.; Greenzweig, Y.; Notte, J.; McVey, S. *J. Vac. Sci. Technol. B* **2009**, *27*, 3244.
(32) Zhong, M.; Yang, L.; Shen, H.; Liu, W.; Xiang, X.; Zheng, W.; Guo, D.; Huang, J.; Sun, K.; Yuan, X. *Nucl. Instrum. Methods Phys. Res., Sect. B* **2015**, *353*, 21.
(33) Deng, H.-X.; Li, S.-S.; Li, J. *J. Phys. Chem. C* **2010**, *114*, 4841−4845.
(34) Zhou, W.; Umezawa, N. *Phys. Chem. Chem. Phys.* **2015**, *17*, 17816−17820.
(35) Varley, J. B.; Schleife, A.; Janotti, A.; van de Walle, C. G. V. *Appl. Phys. Lett.* **2013**, *103*, 082118.

DOI: 10.1021/acs.nanolett.5b04815
Nano Lett. XXXX, XXX, XXX−XXX